

# **Title: Holocene warming drove long-term methane increases in lakes across Greenland**

**Authors:** J.M. McFarlin<sup>1,2\*</sup>, Y. Axford<sup>1</sup>, S. Kusch<sup>3</sup>, A. L. Masterson<sup>1</sup>, G.E. Lasher<sup>1,4</sup>, M.R. Osburn<sup>1</sup>

## **Affiliations:**

<sup>1</sup>Department of Earth and Planetary Sciences, Northwestern University, Evanston, Illinois.

<sup>2</sup>Department of Geological Sciences, Institute of Arctic and Alpine Research, University of Colorado Boulder, Boulder, Colorado.

<sup>3</sup>CologneAMS—University of Cologne Centre for Accelerator Mass Spectrometry, University of Cologne, Cologne, Germany.

<sup>4</sup>Department of Geology and Environmental Science, University of Pittsburgh, Pittsburgh, Pennsylvania

\*jamie.mcfarlin@colorado.edu.

## **Summary**

Widespread Arctic lakes are a major natural source of atmospheric methane (CH<sub>4</sub>). Constraining future CH<sub>4</sub> emissions from Arctic lakes requires accounting for carbon-climate feedbacks that develop in lakes with sustained warming<sup>1,2</sup>. Sedimentary archives that extend through prior warm periods can reveal carbon-climate feedbacks that are not fully apparent in modern observations, but information on past lake CH<sub>4</sub> cycling is limited in Arctic settings<sup>3</sup>. To address this key gap, we reconstruct lake CH<sub>4</sub> dynamics through the Holocene in five spatially widespread lakes on Greenland. We find evidence for substantial increases in lake methanogenesis and CH<sub>4</sub> storage in hypolimnetic water in three of these lakes that persisted for thousands of years following relatively modest Holocene warming. Independent biomarker data reveals that Holocene changes in lake CH<sub>4</sub> are tightly related to primary production and lake redox conditions. We infer past changes in lake CH<sub>4</sub> using the hydrogen isotopes of aquatic moss waxes which demonstrate uptake of CH<sub>4</sub>-derived hydrogen in the middle Holocene, likely supplied by moss-associated methanotrophic bacterial colonies<sup>4,5</sup> that expanded as these lakes become increasingly stratified. These Holocene data indicate that ongoing warming of the Arctic will drive long-lasting physical and biologic changes that increase CH<sub>4</sub> in Greenland lakes and widespread Arctic lakes more broadly, as already seen at our northernmost study site.

## **Abstract**

Methane (CH<sub>4</sub>) emissions from Arctic lakes are of global concern in a warming world. Holocene warming provides an opportunity to examine carbon-climate feedbacks that develop over hundreds to thousands of years of warming, but thus far records that document changes in lake CH<sub>4</sub> dynamics in the Arctic are limited. Here, we show that Holocene warming led to widespread increases in CH<sub>4</sub> in Greenland lakes during the middle Holocene driven by increases in primary production and decreases in oxygen in hypolimnetic water due to stratification. We infer changes in CH<sub>4</sub> dynamics using  $\delta^2\text{H}$  values of

sedimentary moss biomarkers which demonstrate at multiple sites on Greenland a several-thousand-year period during which  $\delta^2\text{H}_{\text{moss}}$  values are consistent with uptake of  $\text{CH}_4$ -derived H, likely via intracellular  $\text{H}_2\text{O}$  and  $\text{NH}_4^+$  supplied by endophytic methanotrophic bacteria that dominated in increasingly stratified lakes. These data indicate ongoing warming will promote an enduring shift towards conditions that enhance methanogenesis and increase  $\text{CH}_4$  in warming Arctic lakes whose geometries are prone to thermal stratification even in lakes where these conditions do not exist today. This work also draws attention to a likely role of common aquatic mosses as an important sink of  $\text{CH}_4$  in lakes across the Arctic.

## Main Text

Lakes are a significant natural source of the potent greenhouse gas methane ( $\text{CH}_4$ )<sup>1</sup>. Arctic and boreal landscapes, which are warming at an unprecedented rate<sup>2</sup>, have the highest density of lakes in the world<sup>6</sup>.  $\text{CH}_4$  dynamics in northern lakes are sensitive to temperature<sup>1,7</sup> and warming-driven feedbacks are expected to augment  $\text{CH}_4$  emissions over the coming century<sup>1,8,9</sup>. However, forecasting these emissions remains challenging<sup>10</sup>. Incomplete accounting for increased  $\text{CH}_4$  from Arctic lakes contributes to substantial uncertainty in projecting the global radiative budget over the coming century<sup>2</sup>.

Geologic records of insolation-driven warmth and its consequences in the early to middle Holocene (11,700 to 4,200 years ago) provide unique opportunities to observe long-term shifts in Arctic lake systems in response to sustained warming. The contributions from Arctic lakes to the Holocene  $\text{CH}_4$  budget are poorly quantified relative to those from tropical and boreal wetlands<sup>11,12</sup>. The C and H isotopic composition of atmospheric  $\text{CH}_4$  preserved in ice cores suggest that emissions from Arctic lakes increased during the middle Holocene, despite low global  $\text{CH}_4$  emissions<sup>12,13</sup>. However, Holocene  $\text{CH}_4$  dynamics are not well-constrained because few proxy methods are known to record  $\text{CH}_4$  dynamics in lake systems<sup>3</sup>. Here, we reconstruct Holocene  $\text{CH}_4$  dynamics in multiple lakes across Greenland using the hydrogen (H) isotopic composition of sedimentary plant waxes. Although this proxy is best known for its strong empirical relationship to meteoric water globally<sup>14</sup>, we infer that a symbiosis between aquatic mosses and methanotrophic microbes can strongly influence the H isotopic composition of aquatic moss derived sedimentary waxes<sup>4,5</sup>, far overwhelming the signal from meteoric water during periods of intensified  $\text{CH}_4$  cycling.

Aquatic brown mosses (Class: Bryopsida, Family: Amblystegiaceae) are major components of Arctic lake vegetation<sup>15</sup>. A symbiotic relationship between both *Sphagnum* (Class: Sphagnopsida, Family: Sphagnaceae) and brown mosses and methanotrophic bacteria is well-documented<sup>4,5,16</sup>. Moss-associated methane-oxidizing bacteria (MAMO) form dense colonies within moss cells and on moss surfaces<sup>5</sup>, where they oxidize  $\text{CH}_4$  using  $\text{O}_2$  produced by photosynthesis, and in turn provide the moss  $\text{CO}_2$  and  $\text{H}_2\text{O}$ <sup>4,5,17,18</sup>. Additionally, MAMO also directly supply moss nitrogen (N) by converting  $\text{N}_2$  to plant available ammonium ( $\text{NH}_4^+$ )<sup>19</sup>. Because lacustrine  $\text{CH}_4$  is very  $^2\text{H}$ -depleted relative to meteoric water (commonly  $\sim -250\%$  relative to growth water)<sup>20</sup> due to strong discrimination against heavy isotopes during methanogenesis, H derived from methanotroph-produced  $\text{H}_2\text{O}$  and  $\text{NH}_4^+$  in the intracellular water pool will significantly influence the H isotopic composition of synthesized biomass. Data from Siberian ponds has demonstrated that 60-99% of the  $\text{CH}_4$  produced by sedimentary methanogens in anoxic ponds is oxidized within aquatic brown moss layers<sup>21</sup> demonstrating MAMO are highly efficient at consuming  $\text{CH}_4$  in the water column. This moss-methanotroph symbiosis, along with the widespread abundance of brown mosses in Arctic lakes, is an unexplored source of depletion in sedimentary wax H isotopes and likely to record a signature of  $\text{CH}_4$  dynamics in Arctic lakes. Sedimentary plant waxes are broadly source-

specific by chain-length, with long-chain ( $> n\text{-C}_{25}$ ) waxes primarily from terrestrial vascular plants and mid-chain waxes ( $n\text{-C}_{20} < n\text{-C}_{25}$ ) produced abundantly by mosses<sup>22–24</sup>. This allows us to compare the H isotopic composition of water used by terrestrial vascular plants to that used by aquatic mosses, the former serving as a baseline by which to evaluate influence of  $\text{CH}_4$  that derives from  $\text{CH}_4$  in the latter.

We reconstruct Holocene precipitation isotopes and  $\text{CH}_4$  cycling in five Greenland nonglacial lakes spanning  $\sim 15^\circ$  of latitude (Fig. 1) using isotope and biomarker data. We present new wax H isotope records from Wax Lips Lake (WLL)<sup>25</sup> and Trifna Sø (TS)<sup>26</sup> and revisit records previously published from Lake N3 (N3)<sup>27,28</sup>, Pluto Lake (PL)<sup>28,29</sup>, and Flower Valley Lake (FVL)<sup>30</sup>. We estimate past H isotopic composition of precipitation ( $\delta^2\text{H}_{\text{precip}}$ ) using  $\delta^2\text{H}$  values of long-chain sedimentary waxes, calibrated for plant wax-water fractionation during wax synthesis using global average apparent fractionation factors ( $\epsilon_{\text{app}}$ ,  $-121 \pm 18\text{‰}$  for alkanes,  $-99 \pm 32\text{‰}$  for acids)<sup>14</sup>. We reconstruct  $\delta^2\text{H}$  of aquatic moss growth water ( $\delta^2\text{H}_{\text{moss}}$ ) using  $\delta^2\text{H}$  values of mid-chain sedimentary waxes assuming constant fractionation factors to long-chain waxes and calibrated for wax-water fractionation as above (Methods). All lakes in this compilation are small ( $< 1 \text{ km}^2$ ) and through-flowing and have been isolated from glacial meltwater since their deglaciation in the early Holocene (except for a brief discrete period in the late Holocene at WLL)<sup>25</sup>. Macrofossils of aquatic brown mosses are abundant in cores from WLL, TS, N3, and PL and today form dense mats on the sediment surfaces<sup>25–28</sup>. We additionally reconstruct the isotopic composition of lake water at WLL using the oxygen (O) isotopic composition of an obligate aquatic insect larvae (chironomid;  $\delta^{18}\text{O}_{\text{chiron}}$ ) which grows year-round, calibrated for biosynthetic fractionation<sup>31,32</sup>. We convert estimates of  $\delta^{18}\text{O}_{\text{lake}}$  to  $\delta^2\text{H}_{\text{lake}}$  using the local meteoric water line<sup>33</sup>. This provides an independent estimate of the isotopic composition of lake water to compare against  $\delta^2\text{H}_{\text{moss}}$  at this site.

We find, in agreement with prior publications, that vascular (long-chain) plant waxes at TS, N3, PL, and FVL reflect regional precipitation isotopes through the Holocene (Fig. 2), following multi-millennial trends similar to those of elevation-corrected oxygen isotope values from the Agassiz and Renland ice caps ( $\delta^{18}\text{O}_{\text{ice}}$ ; Fig. 2G)<sup>34,35</sup>. WLL vascular plant waxes show anomalous enrichment during the late Holocene compared with ice cores and vascular plant waxes at all other study lakes. Given that relatively enriched  $\delta^2\text{H}_{\text{precip}}$  values in the late Holocene are not apparent in any other water isotope record from Greenland, the late Holocene trend at WLL likely resulted from a localized change in the source of plant waxes (e.g. increased representation of aerially-transported waxes from lower latitudes)<sup>14</sup> and/or a major change in terrestrial plant growing conditions (e.g. cold summer temperatures, strong aridity), rather than a change in isotopes of precipitation<sup>36</sup>.  $\delta^2\text{H}_{\text{precip}}$  values at TS, WLL, N3, and PL gradually decline through the Holocene, with the strongest amplitude change at the northernmost site TS and lower amplitude trends at N3 and PL. No temporal trend is apparent at the southernmost site FVL. The diminishing amplitude of change in  $\delta^2\text{H}_{\text{precip}}$  values by latitude is consistent with Holocene temperature reconstructions across Greenland, which show the strongest summer warming (up to  $\sim +5^\circ\text{C}$  relative to modern averages) in the northernmost regions (Fig. 2F)<sup>37</sup>.

$\delta^2\text{H}_{\text{moss}}$  values inferred from  $n\text{-C}_{23}$  alkanes,  $n\text{-C}_{21}$  alkanes, and  $n\text{-C}_{24}$  alkanoic acids at TS, WLL, and N3, respectively, are exceptionally  $^2\text{H}$ -depleted in the early-middle Holocene (Fig. 2A,B,C). The exact timing and duration of this depletion varies between TS ( $\sim 7.5 - 3 \text{ ka}$ ), WLL ( $\sim 10 - 2.5 \text{ ka}$ ), and N3 ( $\sim 7.5 - 3 \text{ ka}$ ), but at all three sites the depletion event persists for at least a few thousand years before a shift towards agreement with  $\delta^2\text{H}_{\text{precip}}$  values in the late Holocene. We find that changes in precipitation isotopes are not a viable explanation for this depletion: These  $\delta^2\text{H}_{\text{moss}}$  values can only be produced by integration of a H source that is extremely  $^2\text{H}$ -depleted relative to the range of modern Greenland precipitation from any season. Differences between  $\delta^2\text{H}$  values of mid- and long-chain plant waxes reach extremes of  $\sim 160\text{‰}$ ,  $\sim 170\text{‰}$ , and  $\sim 180\text{‰}$  at TS, WLL, and N3 respectively. While some variability

occurs in the timing and duration of the signal across records, all locations show similar large differences. A mechanism invoked in the literature to explain divergent H isotope trends in mid- vs. long-chain plant waxes, and that published for N3, is changing seasonality of precipitation (e.g. increased winter precipitation)<sup>27,28,38,39</sup>. However, modern seasonal extremes in precipitation  $\delta^2\text{H}$  values at each site differ by ~80-90‰ at N3 and TS, and ~130‰ at WLL (Fig. 2A,B,C)<sup>33,40,41</sup>. Thus, this mechanism fails to achieve observed depletions in  $\delta^2\text{H}_{\text{moss}}$  values at TS, WLL, and N3 when tested in an isotope mass balance model (Methods). Even when we apply a climatically improbable input of 100%  $\delta^2\text{H}_{\text{winter}}$  end-member values as lake water at peak  $^2\text{H}$ -depletion and allow for  $1\sigma$  variability in our fractionation factor based on calibration data ( $\pm 18\text{‰}$  for alkanes,  $\pm 32\text{‰}$  for acids)<sup>14</sup>, our isotope model still yields  $\delta^2\text{H}$  values at least ~30-60‰ more enriched than the most depleted  $\delta^2\text{H}_{\text{moss}}$  values at TS and N3 (Methods; Extended Data Figure S1). Our most extreme model does barely achieve the  $\delta^2\text{H}$  values observed at WLL, but this model is contradicted by our independent estimates of the isotopic composition of lake water at WLL using chironomid larvae, which do not show any trend towards depleted values during the early and middle Holocene despite that this proxy incorporates lake water year-round (Fig. 2B). The viability of the extreme model (i.e. lake water taken up by moss = 100% winter endmember precipitation) at any site is also challenged by independent precipitation archives: there is no concurrent signal of increased winter precipitation incorporated in  $\delta^{18}\text{O}_{\text{ice}}$  values from nearby ice core sites which accumulate precipitation throughout the year. Instead,  $\delta^{18}\text{O}_{\text{ice}}$  was least depleted in the early-middle Holocene (Fig. 2G)<sup>34,35</sup>. Furthermore, the between-site similarity of depletion in  $\delta^2\text{H}_{\text{moss}}$  values, especially between TS and N3, suggests a consistent mechanism, despite the distance between the sites and markedly different climate and precipitation regimes<sup>42,43</sup>.

The observed  $^2\text{H}$ -depletion in  $\delta^2\text{H}_{\text{moss}}$  values in the middle Holocene at TS, WLL, and N3 requires a distinct source of extremely  $^2\text{H}$ -depleted H that can be integrated directly into mid-chain plant waxes but does not affect long-chain waxes at these sites. We posit that MAMO residing within and/or on moss tissues supply  $^2\text{H}$ -depleted hydrogen via methane oxidation using  $\text{CH}_4$  from the water column. Short-term culturing experiments documenting this symbiosis using  $^{13}\text{C}$ -labelled  $\text{CH}_4$  have shown that conservatively 30% to 40% of C in new biomass in *Sphagnum* and *Scorpidium* respectively is derived from  $\text{CH}_4$ <sup>4,5</sup>.  $\text{CH}_4$ -derived C is most strongly incorporated in submerged mosses (compared to aerial mosses) regardless of the species<sup>17,18,44</sup>. To our knowledge, no study has examined if  $\text{CH}_4$ -derived H is incorporated into moss biomass; however, because this symbiosis primarily occurs intracellularly, we postulate that H from  $\text{CH}_4$ -derived  $\text{H}_2\text{O}$  and metabolites including  $\text{NH}_4^+$  supplied by MAMO contribute to the intracellular water pool used by the moss for biosynthesis. Recent studies show substantial rapid uptake of  $\text{CH}_4$  and  $\text{N}_2$  in submerged mosses with methanotrophic symbionts<sup>19</sup> supporting this hypothesis.

Independent proxy evidence from TS in northeast Greenland indicates low hypolimnetic oxygen and supports increased methanogenesis during the middle Holocene period of depleted  $\delta^2\text{H}_{\text{moss}}$  values (Fig. 3). GDGT-0:crenarchaeol (implying strong archaeal methanogenesis) increased<sup>45,46</sup>, as did the fractional abundance of bacterial brGDGT-IIIa<sup>47</sup> and the HP5 index<sup>48</sup> (implying a drop in  $\text{O}_2$  and a shift in lake redox conditions) (Fig. 3B,C,D). The middle Holocene drop in hypolimnetic oxygen and increase in methanogenesis at TS was accompanied by elevated aquatic invertebrate and terrestrial plant macrofossil abundances, indicating a rise in local primary productivity and consequent greater supply of organic matter to sediments (Fig. 3E,F)<sup>26</sup>. Trends in  $\delta^2\text{H}_{\text{C}_{23}}$  values are highly anti-correlated ( $r = -0.7$  to  $-0.8$ ,  $p < 0.001$ ) to the trends in these sedimentary indicators but are not related to trends in  $\delta^2\text{H}_{\text{C}_{29}}$  values (Methods; Extended Data Fig. S2). Thus, multiple lines of evidence strongly support that the conditions required for a moss-methanotroph symbiosis to be favored at TS occurred during the period when we hypothesize moss uptake of  $\text{CH}_4$ -derived H. We note that proxy evidence from the youngest sediment

sampled from TS yields patterns akin to those of the middle Holocene: depleted  $\delta^2\text{H}_{\text{moss}}$  values and a rise in the abundance of biomarkers associated with methanogenesis and methanotrophy, suggesting modern warming-driven changes are shifting  $\text{CH}_4$  dynamics at this northernmost site currently<sup>42</sup>.

Not all sites in this dataset show extremely depleted  $\delta^2\text{H}_{\text{moss}}$  values or (therefore) moss-associated methane oxidation (e.g., PL, FVL). Consistently, only lakes with moss reported as an abundant constituent in core material (i.e. all lakes here except FVL, which does not report isotope data for chain-lengths  $< \text{C}_{25}$ ) and lakes with geometries prone to thermal stratification in the summer demonstrate uptake of  $\text{CH}_4$ -derived H in  $\delta^2\text{H}_{\text{moss}}$  values.  $\text{CH}_4$  production and storage in northern lakes is controlled seasonally by different mechanisms: in relatively deep lakes ( $> \sim 3\text{m}$ ) with small surface areas ( $< 1\text{km}^2$ ) and high nutrient loads,  $\text{CH}_4$  concentrations increase in the hypolimnion in the summer months when lakes are thermally stratified and thus  $\text{O}_2$  limited<sup>49</sup>. Shallow lakes and those with a large surface area, which promotes wind-driven mixing, are less likely to stratify in the summer. The thickness of the hypolimnion in summer-stratified Arctic lakes increases when light penetration depth decreases as lakes become more productive<sup>50</sup>, and additionally increases with higher water temperatures and longer ice-free seasons which strengthen thermal stratification<sup>50–52</sup>. Moss photosynthesis is light limited in the Arctic winter<sup>53</sup> and therefore MAMO are likely to thrive in lakes during the summer where and when stratification develops and  $\text{CH}_4$  concentrations peak. These requisites predict which lakes in our dataset demonstrate incorporation of  $\text{CH}_4$ -derived H in moss biomarkers during the middle Holocene (TS, WLL, and N3, with maximum water depths of  $\sim 6$ , 9, and 16m respectively), and which lakes do not (PL, the shallowest lake in this dataset, with maximum water depth of  $\sim 4\text{m}$ ).

Precipitation isotopes at all sites, as inferred from long-chain vascular plant waxes, follow the broad, insolation-driven pattern of long-term multi-millennial cooling through the Holocene. Although peak summer warmth probably occurred in the early Holocene across most of Greenland, summer temperatures remained elevated above the modern day through the middle Holocene, and primary production at many sites peaked during the warm middle Holocene following several millennia of post-glacial species colonization and succession, and watershed evolution<sup>37</sup>. We find that the middle Holocene combination of warmth and elevated aquatic productivity was accompanied by major shifts in lake  $\text{CH}_4$  cycling in multiple sectors of Greenland. Mechanistically, we postulate that a combination of higher summer air and water temperatures and the attendant longer ice-free seasons paired with greater primary production contributed to more persistent summer stratification of TS, WLL, and N3 during the middle Holocene, when solubility of  $\text{O}_2$  was also lower and delivery of nutrients and organic matter to lakes was higher, and that these conditions promoted methanogenesis, increased  $\text{CH}_4$  storage in the hypolimnion, and favored MAMO (Fig. 4). Major shifts in lake  $\text{CH}_4$  dynamics followed as little as  $+1\text{--}3^\circ\text{C}$  summer warming relative to today (i.e. peak Holocene warmth at N3) but required a prolonged period of warming that allowed primary productivity to develop within these watersheds.

Strong incorporation of  $\text{CH}_4$ -derived H into aquatic moss biomass at TS, WLL, and N3 during the middle Holocene demonstrates that  $\text{CH}_4$  dynamics drastically changed in widespread lakes across Greenland for thousands of years during the last period of prolonged warmth and greening across Greenland. Elevated methanogenesis in these Arctic lakes occurred when global  $\text{CH}_4$  production was at a Holocene low and points to why  $\text{CH}_4$  emissions decreased more strongly in the tropics than the Arctic, despite a reduction in methanogenesis from boreal peatlands<sup>13</sup>. Incorporation of  $\text{CH}_4$ -derived H into aquatic moss biomass, and thus inferred methanogenesis and water column storage of  $\text{CH}_4$ , decreased at all three affected study sites with summer cooling of  $\sim 1\text{--}3^\circ\text{C}$  in the late Holocene revealing an important climate dependence on Arctic lake  $\text{CH}_4$  cycling. At TS, modern biomarker data indicate this lake is already beginning to transition to a state of enhanced  $\text{CH}_4$  cycling, similar to the middle Holocene. This

paleolimnological perspective from the Holocene suggests that ongoing warming and extension of the ice-free season, paired with predicted increases in aquatic primary production, will drive major increases in lake CH<sub>4</sub> in widespread Greenland lakes and Arctic lakes more broadly and thus higher emissions potential over the coming centuries. In many of these high-latitude lakes, our results also suggest that the widespread presence of aquatic mosses may act as a quantitatively important sink for CH<sub>4</sub>—pointing to a complex role for Arctic lakes in the future global carbon cycle.

## Methods

### *Sedimentary Waxes Concentration, and Hydrogen and Carbon Isotopic Composition*

WLL sediment cores were refrigerated at 4°C for ~1 year prior to subsampling for biomarker analyses. Lipids were extracted from 0.5-3 g of lyophilized sediment using a MARS Microwave Extractor<sup>TM</sup> in 9:1 DCM: MeOH. The extraction program included a 5-minute ramp to 100°C, 20-minutes at 100°C, and a minimum of 30-minute cool down period. Total lipid extracts (TLEs) were filtered and saponified in 0.5 NaOH at 70°C for 8-12 hours, then acidified and separated from the aqueous phase using Methyl-Tert-Butyl ether (MTBE) 3x. TLEs were then separated into fractions (alkanes, alcohols, acids) using Discovery (Sigma Aldrich) amino-propyl solid phase extraction (SPE) columns sequentially eluting with Hexane, 9:1 DCM: Acetone, 2.5% formate in DCM respectively. Saturated alkanes were separated from unsaturated alkanes using Discovery (Sigma Aldrich) Ag-ion SPE columns, Hexane, and Acetone. Sediment storage, preparation, and lipid extraction for Trifna Sø (TS) is discussed in Kusch et al (2019)<sup>26</sup>.

Alkanes were quantified via gas chromatography using a Thermo Scientific Trace 1310 gas chromatograph (GC) with a ZB5 30m x 0.25 mm ID x 0.25 µm film thickness (Zebron) column coupled to Flame Ionization Detector (FID) and a Thermo DSQ single quadrupole mass spectrometer. The GC program used for quantification ramped oven temperatures at 6°C/minute from 100°C to 330°C. Alkanes were identified via diagnostic mass spectra, comparison to the NIST and in-house libraries, and retention times relative to laboratory standard compounds. Concentrations were calculated from FID peak areas through comparison to that of a 10 µg palmitic acid isobutyl ester (PAIBE) internal quantification standard.

Compound specific carbon (<sup>13</sup>C/<sup>12</sup>C) and hydrogen (<sup>2</sup>H/H) isotope analyses were conducted via GC isotope ratio mass-spectrometry (GC-IRMS) using a Thermo Scientific Trace GC with a ZB5-5MS 30m x 0.25 mm ID x 1 µm film thickness column coupled to a Thermo Delta V Plus IRMS via a pyrolysis (P) or combustion (C) interface and controlled by a Thermo GC-C III via Isodat. Reactions for GC-Pyrolysis-Compound Specific Isotope Analysis (GC-P-CSIA) occurred in an alumina column held at 1420°C with a flow of 1.4 mL/min. Reactions for GC-Combustion-CSIA (GC-C-CSIA) occurred in an oxidizing reactor consisting of a 2XCu/Ni/Pt 0.1 m wire bundle held at 940°C. Tank calibration to the VSMOW and VPDB-LSVEC scales utilized a C<sub>16</sub>-C<sub>30</sub> *n*-alkane standard (A6, Arndt Schimmelmann, Indiana University) and a derivatized C<sub>14</sub>-C<sub>20</sub> fatty acid methyl ester mixed standard (F8b, Alex Sessions, Caltech). Instrumental error was assessed via root mean standard error (RMSE) on F8 and A6, which was run between every 3 sample duplicates and averages < 5‰ (alkanes). The H<sub>3</sub><sup>+</sup> factor was determined and applied regularly and averaged 5.214 ppm/nA during the analytical period during 2016 when WLL samples were run and averaged 3.394 ppm/nA during the analytical period during 2019 when TS samples were run. For each sample, the alkane fractions were measured in duplicate for <sup>2</sup>H/H-isotope analyses and for <sup>13</sup>C/<sup>12</sup>C-isotope analyses. Compound-specific δ<sup>2</sup>H and δ<sup>13</sup>C values are reported as average duplicate values on the VSMOW and VPDB-LSVEC scale respectively. Total analytical error presented on δ<sup>2</sup>H

and  $\delta^{13}\text{C}$  values includes the  $1\sigma$  of measurements on each compound peak as well as the instrumental error over the course of all sample measurements, propagated using the root sum of squares (RSS).  $\delta^{13}\text{C}$  values of methylated fatty acids (FAMEs) were corrected for the addition of the methyl group during derivatization via a derivatized phthalic acid of known C isotopic composition.

#### *Oxygen isotopic composition of chironomid head capsules*

Wax Lips Lake (WLL) sediment samples of 4 to 8 ccs (representing 2 cm of core depth) were collected for chironomid  $\delta^{18}\text{O}$  analysis. Each sample was deflocculated in a 10% KOH solution at  $20^\circ\text{C}$  for 30 minutes, then sieved using  $150\ \mu\text{m}$  mesh and DI water and stored in 50 mL Falcon tubes at  $4^\circ\text{C}$  until ready for picking. Chironomid head capsules were manually handpicked and cleaned of any remaining adhering material under a dissecting microscope, then transferred to pre-weighed and oven dried  $3.2 \times 4\ \text{mm}$  lightweight Elemental Microanalysis® silver capsules. On average,  $\sim 100$  head capsules were collected from the pretreated sediment samples for analysis (totaling  $\sim 100\ \mu\text{g}$  analyte material). The filled silver capsules were then freeze dried for 5 days, weighed to determine final mass, and analyzed for  $\delta^{18}\text{O}$  values on a Thermo Scientific™ High Temperature Conversion Elemental Analyzer (TC/EA) coupled to a Thermo Scientific™ Delta V Isotope Ratio Mass Spectrometer (IRMS) via a ConFlo IV A interface in the Northwestern University Stable Isotope Laboratory. The TC/EA pyrolysis was conducted at  $1450^\circ\text{C}$  and standardization to the VSMOW scale was done via calibration with a mixture of organic (e.g., benzoic acid) and inorganic (e.g.,  $\text{BaSO}_4$ ) standards including Benzoic Acid #A (Indiana University) and NBS127, IAEA-SO5, IAEA- SO6. Average precision on standards during the analytical period was  $\pm 0.4\text{‰}$ . Original chironomid  $\delta^{18}\text{O}$  values are reported as per mil (‰) relative to VSMOW.

A down core subset of isolated chironomid samples were also checked for the presence of carbonates using Fourier Transform Infrared Spectroscopy (FT-IR). Individual head capsules were scanned on a Bruker Hyperion 2000 series FT-IR Microscope system between  $600$  and  $4000\ \text{cm}^{-1}$  at 32 times per  $4\ \text{cm}^{-1}$  resolution. Peaks characteristic of carbonate at  $\sim 712$ ,  $\sim 862$  and  $\sim 1440\ \text{cm}^{-1}$  (corresponding to the in-plane bending vibration, the out-of-plane bending vibration and the asymmetric stretching of bonds in a  $\text{CO}_3^{2-}$  molecule<sup>54–56</sup> were not present in the spectra of any samples.

#### *Correction of O chironomid and H wax isotope values to water isotope values*

The  $\delta^2\text{H}$  values of plant wax alkanes and acids are calibrated to water  $\delta^2\text{H}$  values using the global average apparent fractionation factor estimated from  $n\text{-C}_{29}$  alkanes ( $\epsilon_{\text{app}} = -121 \pm 18\text{‰}$ ) and  $n\text{-C}_{28}$  alkanic acids ( $\epsilon_{\text{app}} = -99 \pm 32\text{‰}$ ) from McFarlin et al. (2019)<sup>14</sup>. The  $1\sigma$  error on these calibrations are represented in Fig.2A-E. These calibrations are estimated from sedimentary long-chain waxes but applied to both mid- and long-chain compounds here because there is existing precedent in wax literature to assume the wax-water fractionation factors of aquatic plants are equal to that of terrestrial plants<sup>27,28,30,38,57</sup>. This precedent is supported by the available observations of wax-water fractionation factors in sedimentary waxes which show statistically indistinguishable fractionation factors between mid-chain waxes and lake water ( $\epsilon_{\text{app}} = -121 \pm 50\text{‰}$ ,  $n=46$  for  $n\text{-C}_{23}$  alkanes and  $\epsilon_{\text{app}} = -112 \pm 33\text{‰}$ ,  $n=109$  for  $n\text{-C}_{24}$  alkanic acids in global data compiled by McFarlin et al. (2019)) compared to long-chain waxes and precipitation, albeit with substantially fewer observations of the former<sup>14</sup>. This precedent is also supported by agreement within error of the apparent fractionation values observed in modern aquatic and nonvascular plants<sup>14,24,39,58</sup>. While larger fractionation effects have been observed in some aquatic plants growing in

saline water or heterotrophically in dark conditions<sup>59,60</sup>, neither of these parameters are consistent with aquatic moss growth during the Arctic summer in non-glacial freshwater lakes<sup>15,53</sup>.

The  $\delta^{18}\text{O}$  values of chironomid head capsules are converted to  $\delta^{18}\text{O}$  values of lake water values using a regression from Van Hardenbroek et al. (2018) (Equation 1) with residual standard error on this estimate of 2.4‰<sup>31</sup>.  $\delta^2\text{H}_{\text{lake}}$  values are estimated from  $\delta^{18}\text{O}_{\text{lake}}$  using the local meteoric water line (LMWL) which is constrained using observations recorded in the IAEA-GNIP database from the nearby Pituffuk Station (Thule, ~60 km from WLL) (Equation 2)<sup>33</sup>, with residual standard error on this relationship of 9‰. The error on estimated  $\delta^2\text{H}_{\text{lake}}$  values represented in Fig. 2 is compounded error that includes analytical error on the oxygen isotope measurements of chironomids ( $\pm 0.4\text{‰}$ ), residual standard error on the Van Hardenbroek et al (2018) regression ( $\pm 2.4\text{‰}$ ), both of which are carried over during O to H isotope calculations, and residual standard error on the LMWL ( $\pm 9\text{‰}$ ).

$$\delta^{18}\text{O}_{\text{lake}} = (0.96 * \delta^{18}\text{O}_{\text{chiron}}) - 22.6 \text{ (Equation 1)}$$

$$\delta^2\text{H}_{\text{lake}} = (7.33 * \delta^{18}\text{O}_{\text{lake}}) - 7.1 \text{ (Equation 2)}$$

#### *Water H isotope mass-balance model*

We assume that  $\delta^2\text{H}_{\text{precip}}$  values, estimated from  $\delta^2\text{H}$  values of long-chain plant waxes ( $n\text{-C}_{29}$  alkanes at TS, WLL;  $n\text{-C}_{28}$  acids at N3), are representative of the growth water available during the summer growing season at each site and that this precipitation will also enter the lake.  $\delta^2\text{H}_{\text{precip}}$  values therefore provide one input to lake water at each site and can be used to assess if endmember  $\delta^2\text{H}_{\text{winter}}$  values (i.e. the most depleted winter precipitation isotopes observed in modern monthly data, estimated as -190‰, -220‰, and -260‰ at N3, TS, and WLL respectively; Bowen et al, 2020)<sup>40,41</sup> can fully explain  $\delta^2\text{H}_{\text{moss}}$  values at the most depleted point in the Holocene (Equation 3). We assume that the largest observable absolute difference between mid- and long-chain wax  $\delta^2\text{H}$  values (maximum  $|\epsilon_{\text{terr-aq}}|$  or  $\epsilon_{\text{max}}$ ; estimated using  $n\text{-C}_{23}$  alkanes at TS,  $n\text{-C}_{21}$  alkanes at WLL and  $n\text{-C}_{24}$  acids at N3) represents when the strongest uptake of winter precipitation would have occurred if this were indeed the mechanism driving trends in  $\delta^2\text{H}_{\text{moss}}$  values and allow the model to incorporate 100%  $\delta^2\text{H}_{\text{winter}}$  values at this point in time (0%  $\delta^2\text{H}_{\text{precip}}$  values). We then scale the input of  $\delta^2\text{H}_{\text{winter}}$  values at all other points in time relative to this point based on the epsilon value between mid- and long-chain wax  $\delta^2\text{H}$  values ( $\epsilon_{\text{terr-aq}}$ ) at each point (Equation 3) given the assumption being tested here that differences in  $\epsilon_{\text{terr-aq}}$  throughout the Holocene are a function of the amount of winter input to each lake.

$$\delta^2\text{H}_{\text{lake}} = (n) * \delta^2\text{H}_{\text{winter}} + (1-n) * \delta^2\text{H}_{\text{precip}} \text{ (Equation 3)}$$

$$n = \epsilon_{\text{terr-aq}} / \epsilon_{\text{max}} \text{ (Equation 4)}$$

Due to the uncertainty in the apparent fractionation factor used to calibrate  $\delta^2\text{H}_{\text{wax}}$  values to  $\delta^2\text{H}_{\text{water}}$  values we also allow for a  $1\sigma$  error on this estimate, which is represented in Fig. S1 (Extended Data). Because there is no incorporation of  $\delta^2\text{H}_{\text{precip}}$  values at the point when  $\delta^2\text{H}_{\text{moss}}$  values are the most depleted, the estimates of  $\delta^2\text{H}_{\text{precip}}$  values are somewhat irrelevant to testing if any amount of winter precipitation can fully explain depleted  $\delta^2\text{H}_{\text{moss}}$  values. We find that 100% winter endmember precipitation cannot explain  $\delta^2\text{H}_{\text{moss}}$  values at TS or N3 during the middle Holocene, and that 100% winter endmember precipitation



can only just explain the early to middle Holocene trends at WLL if we apply the largest fractionation factor in our range ( $\epsilon_{\text{app}} = -139\text{‰}$ ). However, full incorporation of only an extreme winter endmember is climatically improbable (e.g. even an average of winter precipitation across all winter months would be substantially less depleted than the winter endmember) and we have also included models that set the maximum uptake of winter endmember precipitation at 75% and 50% (Equation 5, 6).

$$n_{75} = 0.75 * (\epsilon_{\text{terr-aq}} / \epsilon_{\text{max}}) \text{ (Equation 5)}$$

$$n_{50} = 0.50 * (\epsilon_{\text{terr-aq}} / \epsilon_{\text{max}}) \text{ (Equation 6)}$$

These latter models are more climatically probable and yield lake water values that are in closer agreement with the H isotopic composition of mean annual precipitation at each site<sup>33,41,61</sup>. We note that modern lake water  $\delta^2\text{H}$  values at both WLL (-153‰) and N3 (-96‰) are currently strongly summer-biased, suggesting very little retention of any winter precipitation in lake water into the summer months at these sites currently. We unfortunately have no measurements of modern lake water isotopes for TS. The  $\delta^2\text{H}_{\text{lake}}$  values that result from mixing of the two precipitation endmembers we present here demonstrate the improbability that winter precipitation would ever dominate in these lakes, where equal or more precipitation amounts are delivered during the summer season<sup>43</sup> and given the competing input of more enriched summer precipitation during the early-middle Holocene at each site.

#### *CH<sub>4</sub>-derived H<sub>2</sub>O in cellular water*

Intracellular water in aquatic plants and mosses is sourced from lake water and it is thought that methanotrophic symbionts are able to colonize aquatic moss via water transport<sup>4,5</sup>. It is therefore unlikely that the spaces in which MAMO reside are not freely exchanging H<sub>2</sub>O. This presents a challenge for identifying the exact mechanism by which MAMO supplies CH<sub>4</sub>-derived H to aquatic mosses in appreciable amounts. If it were limited to the H<sub>2</sub>O produced during the oxidation of CH<sub>4</sub>, the exchange of CH<sub>4</sub> would need to be 10<sup>5</sup> to 10<sup>6</sup> times more rapid than the exchange of water within the cell, given the molarity of lake water relative to the concentration of CH<sub>4</sub> even in lakes with elevated dissolved CH<sub>4</sub> (~100  $\mu\text{M}$  CH<sub>4</sub>/L)<sup>51</sup>. Prior work has shown that MAMO can oxidize 80  $\mu\text{M}$  CH<sub>4</sub>/g dry plant mass/day<sup>16</sup> and there exists speculation that aquatic mosses have unique carbon concentrating mechanisms given how slowly CO<sub>2</sub> diffuses in water and the inability of these plants to use bicarbonate<sup>62</sup>. To our knowledge, there is no work on aquatic brown mosses that can point to whether or not this mechanism alone is a sufficient explanation. However, there are also additional pathways for CH<sub>4</sub>-derived H to enter the cellular water pool in aquatic mosses via MAMO, including via MAMO supplied ammonium<sup>19</sup>. NH<sub>4</sub><sup>+</sup> assimilation occurs within chloroplasts and therefore could be contributing NH<sub>4</sub><sup>+</sup>-derived H directly to the NADPH pool<sup>63–65</sup>. Understanding of the source of H to NADPH pools and the cycling of NADPH in plants is limited but recognized as a major control on intracellular water and the H isotopic composition of plant lipids<sup>66</sup>.

#### *Compound-specific C isotope measurements*

Measurements on the carbon isotopic composition of some plant wax compounds were performed at WLL (plant wax *n*-alkanes C<sub>21</sub>-C<sub>31</sub>) and TS (*n*-alkanoic acids C<sub>16</sub>, C<sub>20</sub>-C<sub>30</sub>; alkane fractions were

consumed during H isotope analyses) in an effort to document moss uptake of CH<sub>4</sub>-derived C supplied by endophytic methanotrophs. Wax carbon isotopes range from ~ -25 to -37‰ VPBD at WLL, and from ~ -22 to -36‰ VPBD at TS. We publicly archive all carbon isotope data and plot it here along with the sedimentary abundances of these biomarkers (reported by and discussed in Kusch et al, 2019)<sup>26</sup>(Extended Data, Fig. S3, S4). Although depleted CH<sub>4</sub>-derived C isotopes are likely used by moss during photosynthesis along with CH<sub>4</sub>-derived H supplied by MAMO, we find that these measurements neither strongly support nor refute our hypothesis. While there is a moderate depletion trend in carbon isotopes in specifically mid-chain waxes concurrent with the strong depletion trend in H isotopes in these same waxes at both WLL and TS, the most depleted C isotope values that we observe in mid-chain waxes occur in the late Holocene in both records. We also observe that the most depleted C isotope values overall occur in long-chain waxes, while the most enriched C isotope values occur in short-chain waxes (C<sub>16</sub> *n*-alkanoic acids at TS), suggesting strong competing effects within the C pool at each lake. We find that the integration of multiple sources of C into aquatic plant waxes in a lacustrine systems yields a mixing model that is unable to distinguish between the signature of terrestrial C produced during aerobic respiration of organic matter at the sediment interface ( $\delta^{13}\text{C} \sim -25$  to  $-35\text{‰}$ , estimated from values of contemporaneous long-chain plant waxes), CH<sub>4</sub>-derived C from moss-associated methane oxidation ( $\delta^{13}\text{C}_{\text{CH}_4} \sim -50\text{‰}$  to  $-80\text{‰}$ ; Cadieux et al, 2016)<sup>52</sup>, and uptake of the residual DIC-CO<sub>2</sub> pool in lake water that was fractionated during hydrogenotrophic methanogenesis ( $\delta^{13}\text{C}_{\text{CO}_2} \sim 0$  to  $-20\text{‰}$ ; Conrad et al, 2011)<sup>67</sup> which can be as or more common than acetoclastic methanogenesis in lakes<sup>68</sup>. A strongly enriched DIC pool during the early-middle Holocene relative to the late Holocene is supported by trends in  $\delta^{13}\text{C}$  values in C<sub>16</sub> *n*-alkanoic acids at TS.

#### Data availability

All novel data [will be] publicly archived on the NOAA paleoclimate database. R code and all data used in these analyses are also publicly available on Github at <https://github.com/JmMcFarlin/McFarlin-et-al-.git>. Any remaining lipid extracts for WLL and TS are housed at Northwestern University.

#### References

- Wik, M., Varner, R. K., Anthony, K. W., MacIntyre, S. & Bastviken, D. Climate-sensitive northern lakes and ponds are critical components of methane release. *Nat. Geosci.* **9**, 99–105 (2016).
- Collins, M. *et al.* 2013: Long-term Climate Change: Projections, Commitments and Irreversibility. in *Climate Change 2013: The Physical Science Basis. Contribution of Working Group I to the Fifth Assessment Report of the Intergovernmental Panel on Climate Change* 1029–1136 (Cambridge University Press, 2013).
- Sundqvist, H. *et al.* Arctic Holocene proxy climate database—new approaches to assessing geochronological accuracy and encoding climate variables. *Clim. Past* **10**, 1605–1631 (2014).
- Liebner, S. *et al.* Methane oxidation associated with submerged brown mosses reduces methane emissions from Siberian polygonal tundra. *J. Ecol.* **99**, 914–922 (2011).
- Raghoebarsing, A. A. *et al.* Methanotrophic symbionts provide carbon for photosynthesis in peat bogs. *Nature* **436**, 1153–1156 (2005).

- 425 6. Verpoorter, C., Kutser, T., Seekell, D. A. & Tranvik, L. J. A global inventory of lakes based on  
426 high-resolution satellite imagery. *Geophys. Res. Lett.* **41**, 6396–6402 (2014).
- 427 7. Wik, M. *et al.* Energy input is primary controller of methane bubbling in subarctic lakes. *Geophys.*  
428 *Res. Lett.* **41**, 555–560 (2014).
- 429 8. Walter, K. M., Zimov, S. A., Chanton, J. P., Verbyla, D. & Chapin, F. S. Methane bubbling from  
430 Siberian thaw lakes as a positive feedback to climate warming. *Nature* **443**, 71–75 (2006).
- 431 9. Walter, K. M., Smith, L. C. & Chapin, F. S. Methane bubbling from northern lakes: Present and  
432 future contributions to the global methane budget. *Philos. Trans. R. Soc. A Math. Phys. Eng. Sci.*  
433 **365**, 1657–1676 (2007).
- 434 10. Engram, M. *et al.* Remote sensing northern lake methane ebullition. *Nat. Clim. Chang.* **10**, 511–  
435 517 (2020).
- 436 11. Zheng, Y. *et al.* Holocene variations in peatland methane cycling associated with the Asian  
437 summer monsoon system. *Nat. Commun.* **5**, 4631 (2014).
- 438 12. Zheng, Y. *et al.* Operation of the boreal peatland methane cycle across the past 16 k.y. *Geology*  
439 **48**, 82–86 (2020).
- 440 13. Sowers, T. Atmospheric methane isotope records covering the Holocene period. *Quat. Sci. Rev.*  
441 **29**, 213–221 (2010).
- 442 14. McFarlin, J. M., Axford, Y., Masterson, A. L. & Osburn, M. R. Calibration of modern  
443 sedimentary  $\delta^2\text{H}$  plant wax-water relationships in Greenland lakes. *Quat. Sci. Rev.* **225**, 105978  
444 (2019).
- 445 15. Sand-Jensen, K., Riis, T., Markager, S. & Vincent, W. F. Slow growth and decomposition of  
446 mosses in Arctic lakes. *Can. J. Fish. Aquat. Sci.* **56**, 388–393 (1999).
- 447 16. Kip, N. *et al.* Global prevalence of methane oxidation by symbiotic bacteria in peat-moss  
448 ecosystems. *Nat. Geosci.* **3**, 617–621 (2010).
- 449 17. Basiliko, N., Knowles, R. & Moore, T. R. Roles of moss species and habitat in methane  
450 consumption potential in a northern peatland. *Wetlands* **24**, 178–185 (2004).
- 451 18. Zibulski, R. *et al.* C / N ratio, stable isotope ( $\delta^{13}\text{C}$ ,  $\delta^{15}\text{N}$ ), and n-alkane patterns of brown  
452 mosses along hydrological gradients of low-centred polygons of the Siberian Arctic.  
453 *Biogeosciences* **14**, 1617–1630 (2017).
- 454 19. Larmola, T. *et al.* Methanotrophy induces nitrogen fixation during peatland development. *Proc.*  
455 *Natl. Acad. Sci.* **111**, 734–739 (2014).
- 456 20. Chanton, J. P., Fields, D. & Hines, M. E. Controls on the hydrogen isotopic composition of  
457 biogenic methane from high-latitude terrestrial wetlands. *J. Geophys. Res. Biogeosciences* **111**,  
458 (2006).
- 459 21. Knoblauch, C., Spott, O., Evgrafova, S., Kutzbach, L. & Pfeiffer, E. Regulation of methane  
460 production, oxidation, and emission by vascular plants and bryophytes in ponds of the northeast  
461 Siberian polygonal tundra. *J. Geophys. Res. Biogeosciences* **120**, 2525–2541 (2015).
- 462 22. Ficken, K. J., Li, B., Swain, D. L. & Eglinton, G. An n-alkane proxy for the sedimentary input of  
463 submerged/floating freshwater aquatic macrophytes. *Org. Geochem.* **31**, 745–749 (2000).

- 464 23. Gao, L., Hou, J., Toney, J., MacDonald, D. & Huang, Y. Mathematical modeling of the aquatic  
465 macrophyte inputs of mid-chain n-alkyl lipids to lake sediments: Implications for interpreting  
466 compound specific hydrogen isotopic records. *Geochim. Cosmochim. Acta* **75**, 3781–3791 (2011).
- 467 24. Dion-Kirschner, H., McFarlin, J. M., Masterson, A. L., Axford, Y. & Osburn, M. R. Modern  
468 constraints on the sources and climate signals recorded by sedimentary plant waxes in west  
469 Greenland. *Geochim. Cosmochim. Acta* **286**, 336–354 (2020).
- 470 25. McFarlin, J. M. *et al.* Pronounced summer warming in northwest Greenland during the Holocene  
471 and Last Interglacial. *Proc. Natl. Acad. Sci.* **115**, 6357–6362 (2018).
- 472 26. Kusch, S. *et al.* Holocene environmental history in high-Arctic North Greenland revealed by a  
473 combined biomarker and macrofossil approach. *Boreas* **48**, 273–286 (2019).
- 474 27. Thomas, E. K., Briner, J. P., Ryan-Henry, J. J. & Huang, Y. A major increase in winter snowfall  
475 during the middle Holocene on western Greenland caused by reduced sea ice in Baffin Bay and  
476 the Labrador Sea. *Geophys. Res. Lett.* **43**, 5302–5308 (2016).
- 477 28. Thomas, E. K., Hollister, K. V., Cluett, A. A. & Corcoran, M. C. Reconstructing Arctic  
478 Precipitation Seasonality Using Aquatic Leaf Wax  $\delta^2\text{H}$  in Lakes With Contrasting Residence  
479 Times. *Paleoceanogr. Paleoclimatology* **35**, e2020PA003886 (2020).
- 480 29. Axford, Y. *et al.* Holocene temperature history at the western Greenland Ice Sheet margin  
481 reconstructed from lake sediments. *Quat. Sci. Rev.* **59**, 87–100 (2013).
- 482 30. Balascio, N. L., D'Andrea, W. J., Bradley, R. S. & Perren, B. B. Biogeochemical evidence for  
483 hydrologic changes during the Holocene in a lake sediment record from southeast Greenland. *The*  
484 *Holocene* **23**, 1428–1439 (2013).
- 485 31. van Hardenbroek, M. *et al.* The stable isotope composition of organic and inorganic fossils in lake  
486 sediment records : Current understanding , challenges , and future directions. *Quat. Sci. Rev.* **196**,  
487 154–176 (2018).
- 488 32. Lasher, G. E. *et al.* Holocene temperatures and isotopes of precipitation in Northwest Greenland  
489 recorded in lacustrine organic materials. *Quat. Sci. Rev.* **170**, 45–55 (2017).
- 490 33. IAEA/WMO. Global Network of Isotopes in Precipitation. The GNIP Database. (2020).
- 491 34. Lecavalier, B. S. *et al.* High Arctic Holocene temperature record from the Agassiz ice cap and  
492 Greenland ice sheet evolution. *Proc. Natl. Acad. Sci. U. S. A.* **114**, 5952–5957 (2017).
- 493 35. Vinther, B. M. *et al.* Holocene thinning of the Greenland ice sheet. *Nature* **461**, 385–388 (2009).
- 494 36. Kahmen, A. *et al.* Leaf water deuterium enrichment shapes leaf wax n-alkane  $\delta\text{D}$  values of  
495 angiosperm plants II: Observational evidence and global implications. *Geochim. Cosmochim. Acta*  
496 **111**, 50–63 (2013).
- 497 37. Axford, Y., Osterberg, E. C. & de Vernal, A. Past warmth and its impacts in Greenland during the  
498 Holocene Thermal Maximum. *Annu. Rev. Earth Planet. Sci. (in press)*.
- 499 38. Rach, O., Kahmen, A., Brauer, A. & Sachse, D. A dual-biomarker approach for quantification of  
500 changes in relative humidity from sedimentary lipid D/H ratios. *Clim. Past* **13**, 741–757 (2017).
- 501 39. Balascio, N. L., D'Andrea, W. J., Anderson, R. S. & Wickler, S. Influence of vegetation type on n-  
502 alkane composition and hydrogen isotope values from a high latitude ombrotrophic bog. *Org.*

503 *Geochem.* **121**, 48–57 (2018).

504 40. Bowen, G. J., Wassenaar, L. I. & Hobson, K. A. Global application of stable hydrogen and oxygen  
505 isotopes to wildlife forensics. *Oecologia* **143**, 337–348 (2005).

506 41. Bowen, G. J. The Online Isotopes in Precipitation Calculator, version 3.1.  
507 [http://wateriso.utah.edu/waterisotopes/pages/data\\_access/oipc.html](http://wateriso.utah.edu/waterisotopes/pages/data_access/oipc.html) (2020).

508 42. Hanna, E., Mernild, S. H., Cappelen, J. & Steffen, K. Recent warming in Greenland in a long-term  
509 instrumental (1881–2012) climatic context: I. Evaluation of surface air temperature records.  
510 *Environ. Res. Lett.* **7**, 045404 (2012).

511 43. Mernild, S. H. *et al.* Greenland precipitation trends in a long-term instrumental climate context  
512 (1890–2012): evaluation of coastal and ice core records. *Int. J. Climatol.* **35**, 303–320 (2015).

513 44. Larmola, T. *et al.* The role of Sphagnum mosses in the methane cycling of a boreal mire. *Ecology*  
514 **91**, 2356–2365 (2010).

515 45. Blaga, C. I., Reichart, G.-J., Heiri, O. & Sinninghe Damsté, J. S. Tetraether membrane lipid  
516 distributions in water-column particulate matter and sediments: a study of 47 European lakes along  
517 a north–south transect. *J. Paleolimnol.* **41**, 523–540 (2009).

518 46. Lattaud, J., De Jonge, C., Elling, F. J., Pearson, A. & Eglinton, T. I. *Microbial lipid signatures in*  
519 *Arctic deltaic sediments - insight into methane cycling and climate variability.* *Earth ArXiv* (2020)  
520 doi:<https://doi.org/10.31223/X5B01W>.

521 47. Tierney, J. E. GDGT Thermometry: Lipid Tools for Reconstructing Paleotemperatures. in  
522 *Reconstructing Earth's Deep-Time Climate--The State of the Art in 2012* 115–131 (2012).

523 48. Yao, Y. *et al.* Correlation between the ratio of 5-methyl hexamethylated to pentamethylated  
524 branched GDGTs (HP5) and water depth reflects redox variations in stratified lakes. *Org.*  
525 *Geochem.* **147**, 104076 (2020).

526 49. Juutinen, S. *et al.* Methane dynamics in different boreal lake types. *Biogeosciences* **6**, 209–223  
527 (2009).

528 50. Saros, J. E., Northington, R. M., Osburn, C. L., Burpee, B. T. & John Anderson, N. Thermal  
529 stratification in small arctic lakes of southwest Greenland affected by water transparency and  
530 epilimnetic temperatures. *Limnol. Oceanogr.* **61**, 1530–1542 (2016).

531 51. Northington, R. M. & Saros, J. E. Factors Controlling Methane in Arctic Lakes of Southwest  
532 Greenland. *PLoS One* **11**, e0159642 (2016).

533 52. Cadieux, S. B. *et al.* Large fractionations of C and H isotopes related to methane oxidation in  
534 Arctic lakes. *Geochim. Cosmochim. Acta* **187**, 141–155 (2016).

535 53. Riis, T. & Sand-Jensen, K. Growth Reconstruction and Photosynthesis of Aquatic Mosses:  
536 Influence of Light, Temperature and Carbon Dioxide at Depth. *J. Ecol.* **85**, 359–372 (1997).

537 54. Liu, X., Colman, S. M., Brown, E. T., Minor, E. C. & Li, H. Estimation of carbonate, total organic  
538 carbon, and biogenic silica content by FTIR and XRF techniques in lacustrine sediments. *J.*  
539 *Paleolimnol.* **50**, 387–398 (2013).

540 55. Reig, F. FTIR quantitative analysis of calcium carbonate (calcite) and silica (quartz) mixtures  
541 using the constant ratio method. Application to geological samples. *Talanta* **58**, 811–821 (2002).

56. Xia, M., Yao, Z., Ge, L., Chen, T. & Li, H. A potential bio-filler: The substitution effect of  
furfural modified clam shell for carbonate calcium in polypropylene. *J. Compos. Mater.* **49**, 807–  
816 (2015).
57. Curtin, L. *et al.* Holocene and Last Interglacial climate of the Faroe Islands from sedimentary  
plant wax hydrogen and carbon isotopes. *Quat. Sci. Rev.* **223**, 105930 (2019).
58. Aichner, B., Herzschuh, U., Wilkes, H., Vieth, A. & Böhner, J.  $\delta D$  values of n-alkanes in Tibetan  
lake sediments and aquatic macrophytes – A surface sediment study and application to a 16ka  
record from Lake Koucha. *Org. Geochem.* **41**, 779–790 (2010).
59. Yakir, D. & DeNiro, M. J. Oxygen and Hydrogen Isotope Fractionation during Cellulose  
Metabolism in *Lemna gibba* L. *Plant Physiol.* **93**, 325–332 (1990).
60. Aichner, B., Hilt, S., Périllon, C., Gillefalk, M. & Sachse, D. Biosynthetic hydrogen isotopic  
fractionation factors during lipid synthesis in submerged aquatic macrophytes: Effect of  
groundwater discharge and salinity. *Org. Geochem.* **113**, 10–16 (2017).
61. Bowen, G. J. & Revenaugh, J. Interpolating the isotopic composition of modern meteoric  
precipitation. *Water Resour. Res.* **39**, 1–13 (2003).
62. Glime, J. Nutrient Relations: CO<sub>2</sub>. in *Bryophyte Ecology* (2017).
63. Hodges, M., Flesch, V., Gálvez, S. & Bismuth, E. Higher plant NADP<sup>+</sup>-dependent isocitrate  
dehydrogenases, ammonium assimilation and NADPH production. *Plant Physiol. Biochem.* **41**,  
577–585 (2003).
64. Hirel, B. & Lea, P. J. Ammonia Assimilation. in *Plant Nitrogen* 79–99 (Springer Berlin  
Heidelberg, 2001). doi:10.1007/978-3-662-04064-5\_4.
65. Noctor, G. & Foyer, C. H. A re-evaluation of the ATP :NADPH budget during C<sub>3</sub> photosynthesis:  
a contribution from nitrate assimilation and its associated respiratory activity? *J. Exp. Bot.* **49**,  
1895–1908 (1998).
66. Sachse, D. *et al.* Molecular Paleohydrology: Interpreting the Hydrogen-Isotopic Composition of  
Lipid Biomarkers from Photosynthesizing Organisms. *Annu. Rev. Earth Planet. Sci.* **40**, 221–249  
(2012).
67. Conrad, R. *et al.* Stable carbon isotope discrimination and microbiology of methane formation in  
tropical anoxic lake sediments. *Biogeosciences* **8**, 795–814 (2011).
68. Mandić-Mulec, I., Gorenc, K., Petrišič, M. G., Faganeli, J. & Ogrinc, N. Methanogenesis pathways  
in a stratified eutrophic alpine lake (Lake Bled, Slovenia). *Limnol. Oceanogr.* **57**, 868–880 (2012).

## Acknowledgments

We thank the people and Government of Greenland (sample export permit 028/2014), the Thule Air Base, Air Greenland, the US Air Force, the Air National Guard, and Polar Field Services for logistical support. A. Taylor, G. Bromley, M. Jackson, L. Farnsworth assisted in field work. H. Dion-Kirshner, J. Todes, S. Lee provided laboratory assistance. Sebastian Kopf provided helpful feedback on this manuscript. Published data was obtained from the NOAA paleoclimate database. Map was created using The Generic Mapping Tools (GMT). Funding sources include NSF Division of Polar Programs (Awards 1108306,

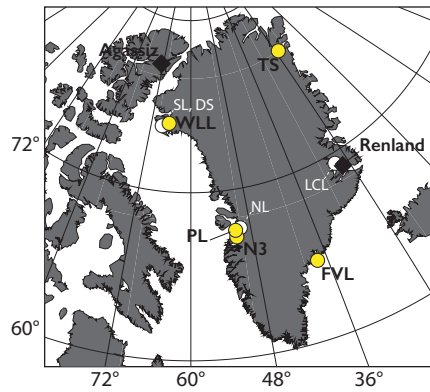
1107411, 1454734), NSF-GRF awarded to J.M.M.; Northwestern University (NU) ISEN Award to Y.A.,  
NU ISEN Award to M.R.O.; GSA Graduate Student Research Award to J.M.M.

**Author contributions:** J.M.M., Y.A., M.R.O. designed research; J.M.M., M.R.O., S.K., G.E.L., A.M.,  
performed research; J.M.M., M.R.O., Y.A., S.K. analyzed data; J.M.M., Y.A., M.R.O., S.K. wrote the  
paper

**Competing Interests:** Authors declare no competing interests.

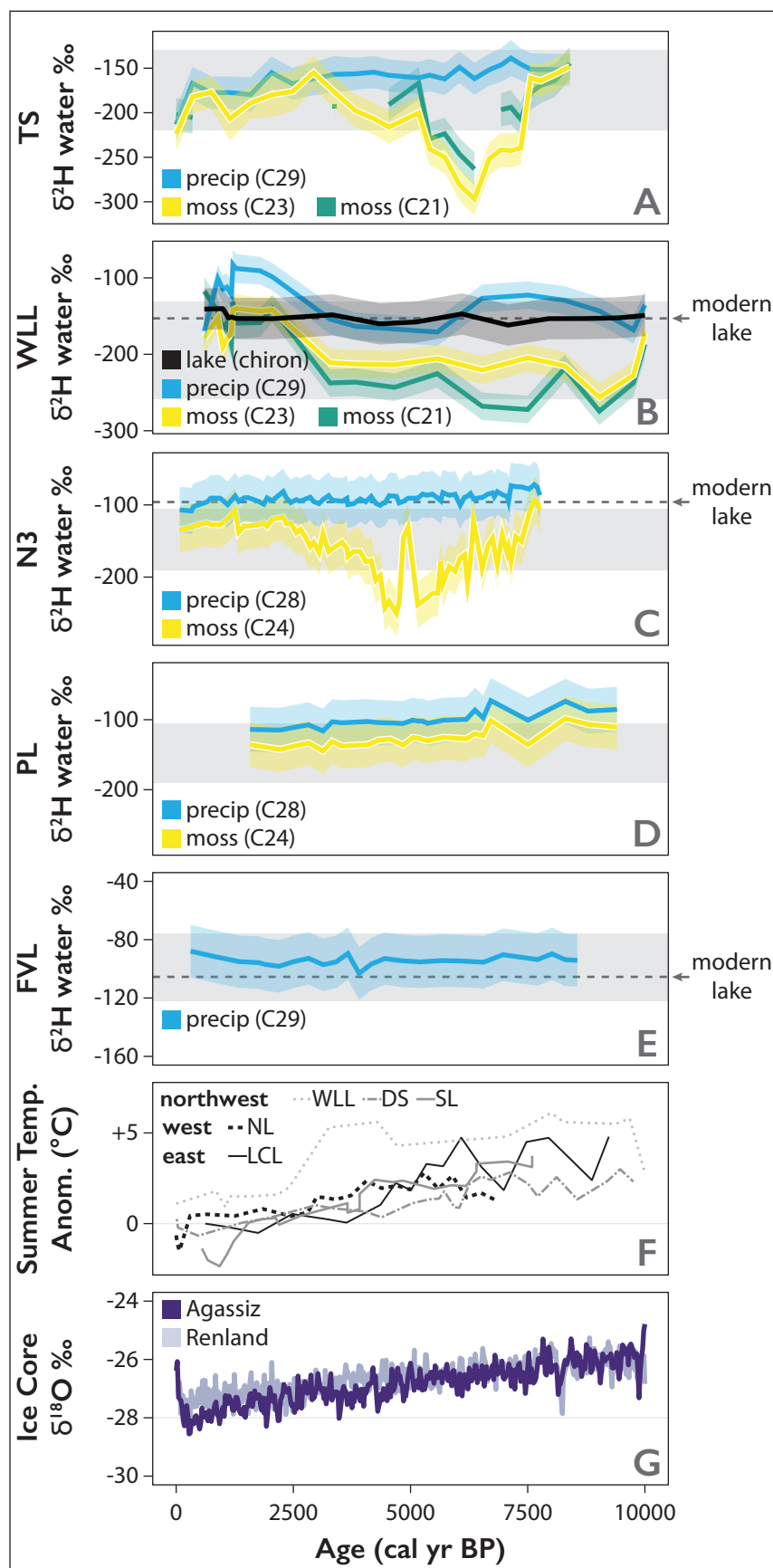
**Materials & Correspondence:** Inquiries regarding this manuscript and material requests should be  
addressed to Dr. Jamie McFarlin at [jamie.mcfarlin@colorado.edu](mailto:jamie.mcfarlin@colorado.edu).

**Figures**



**Figure 1.** Map of Greenland with sites discussed in text. Yellow circles are lakes with sedimentary plant wax isotope data included here. White circles are lakes with select published temperature reconstructions. Black diamonds represent ice core drilling locations for records discussed in this text<sup>34,35</sup>. Lake name abbreviations: WLL= Wax Lips Lake<sup>25</sup>, TS = Trifna Sø<sup>26</sup>, N3 = Lake N3, PL = Pluto Lake<sup>27,28</sup>, FVL = Flower Valley Lake<sup>30</sup>, SL = Secret Lake<sup>32</sup>, DS = Delta Sø, NL = North Lake, LCL = Last Chance Lake<sup>37</sup>.





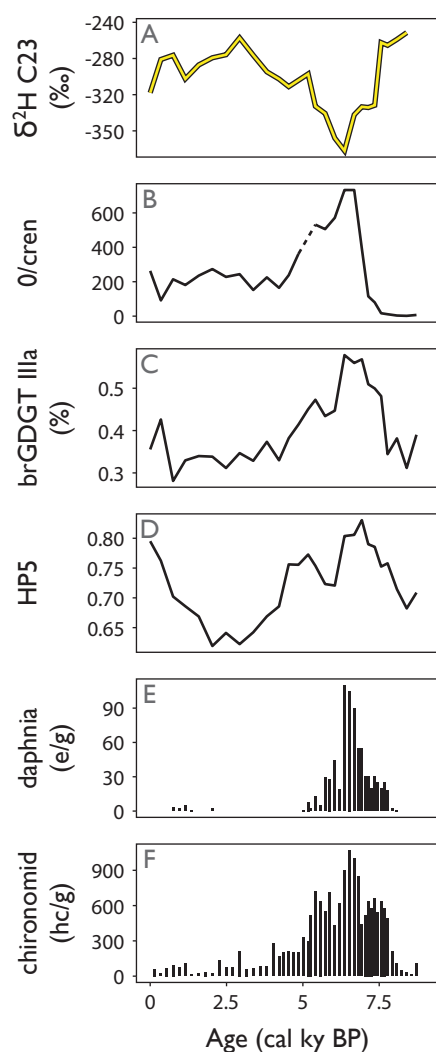


**Figure 3.** Holocene proxy data from TS showing A)  $\delta^2\text{H}_{\text{wax}}$  values of sedimentary mid-chain alkanes, B) ratio of isoGDGT-0:crenarchaeol, C) fractional abundance of brGDGT IIIa (%), the calculated HP5 index of redox state<sup>48</sup>, concentration of D) aquatic invertebrate remains from *Daphnia* in ephippia per gram dry sediment (e/g) and E) chironomid larvae in head capsules per gram dry sediment (hc/g)<sup>26</sup>.

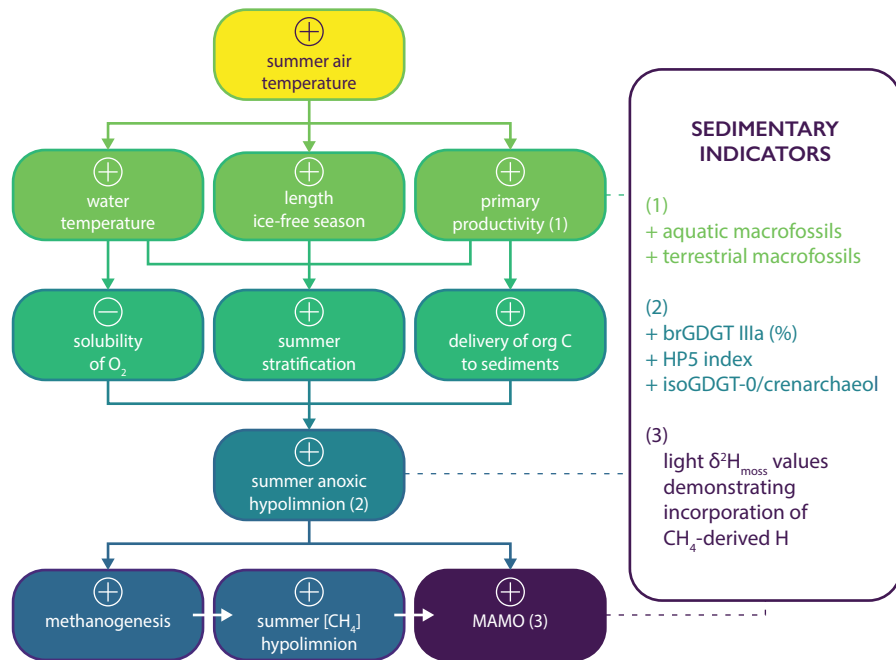


**Figure 4.** Flow chart of the proposed system changes hypothesized for TS, WLL, and N3 forced by warming air temperatures in the early-middle Holocene. Dashed lines identify areas where proxy data from TS provide a sedimentary indicator of that change, with those indicators listed by number in gray panel on the right. + symbols denote an increase or strengthening of variable, - symbol denotes a decrease or weakening of variable,  $[\text{CH}_4]$  = concentration of methane, MAMO = moss-associated methane oxidation.

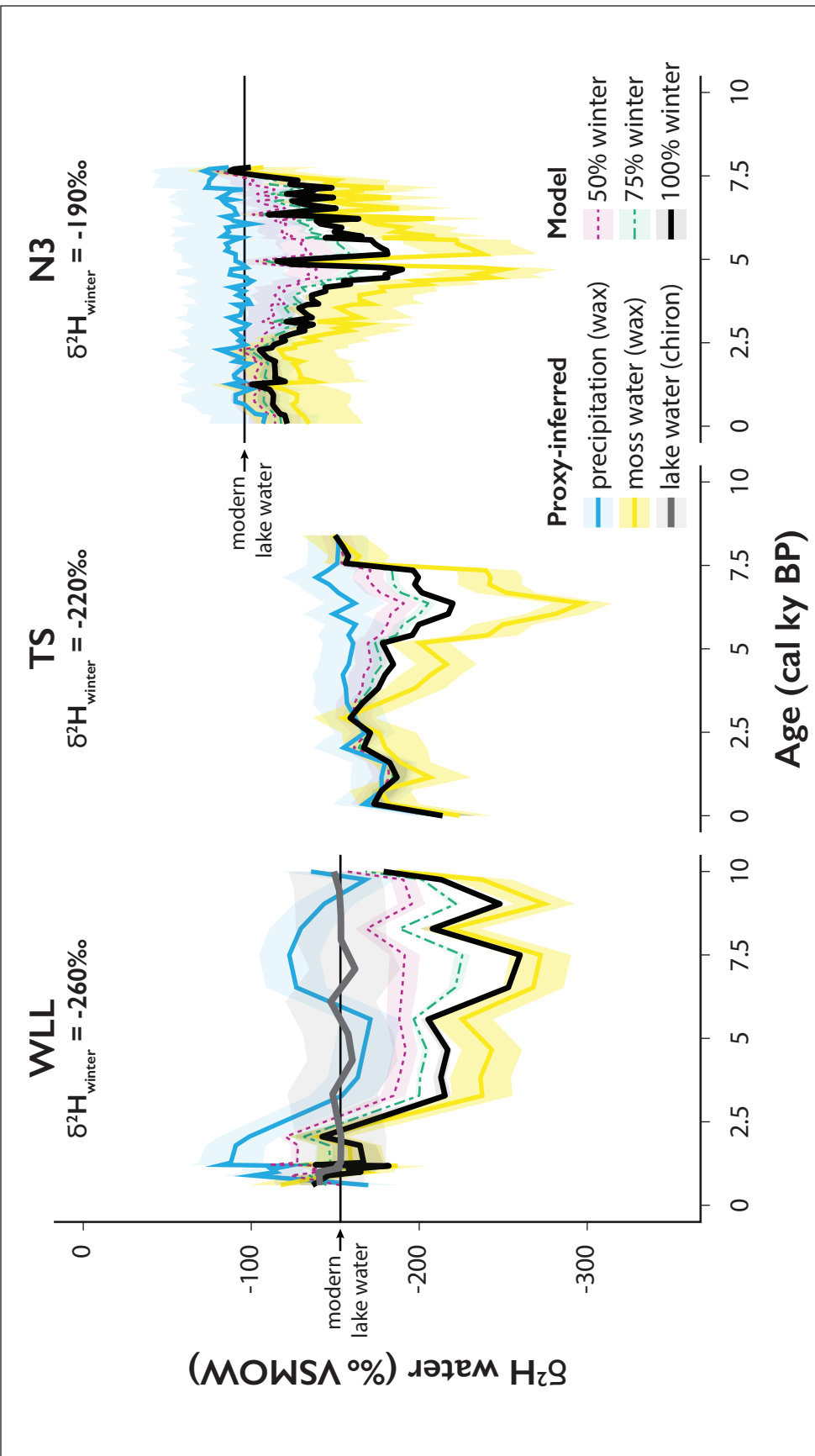
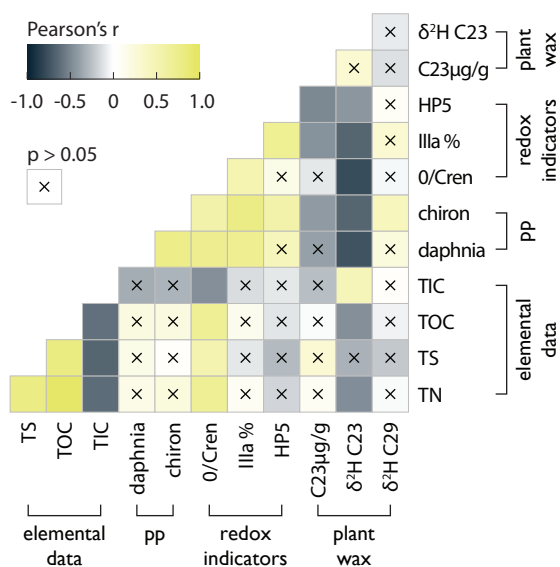


Figure S1. Hydrogen isotope mass balance models for WLL, TS, and N3 demonstrating proxy-inferred  $\delta^2\text{H}$  values of precipitation (blue lines), proxy-inferred  $\delta^2\text{H}$  values of moss water (yellow lines), and modelled  $\delta^2\text{H}$  values of lake water using 100% winter endmember precipitation (black lines), 75% winter endmember precipitation (green dashed lines), and 50% winter endmember precipitation (pink dotted lines) at the point of great offset between precipitation and moss water.



**Figure S2.** Correlation matrix showing Pearson's  $r$  between variables at TS with proxy data grouped by category: elemental data, including total nitrogen (TN), total sulfur (TS), total organic carbon (TOC), and total inorganic carbon (TIC); indicators of primary productivity rates (PP), including abundances of ephippia of *Daphnia* and chironomid head capsules per gram sediment; redox indicators sensitive to hypolimnetic oxygen, including the ratio of isoG-DGT-0/crenarchaeol (0/cren), fractional abundances of brGDGT IIIa as a percent relative to all brGDGT isomers (IIIa %), and the HP5 index (Yao et al, 2020); and plant wax biomarkers, including abundance of C23 n-alkanes in  $\mu\text{g/g}$  TOC, and  $\delta^2\text{H}$  values of C23 and C29 n-alkanes; where dark gray represents  $r = -1$ , white represents  $r = 0$ , and bright yellow represents  $r = 1$ .

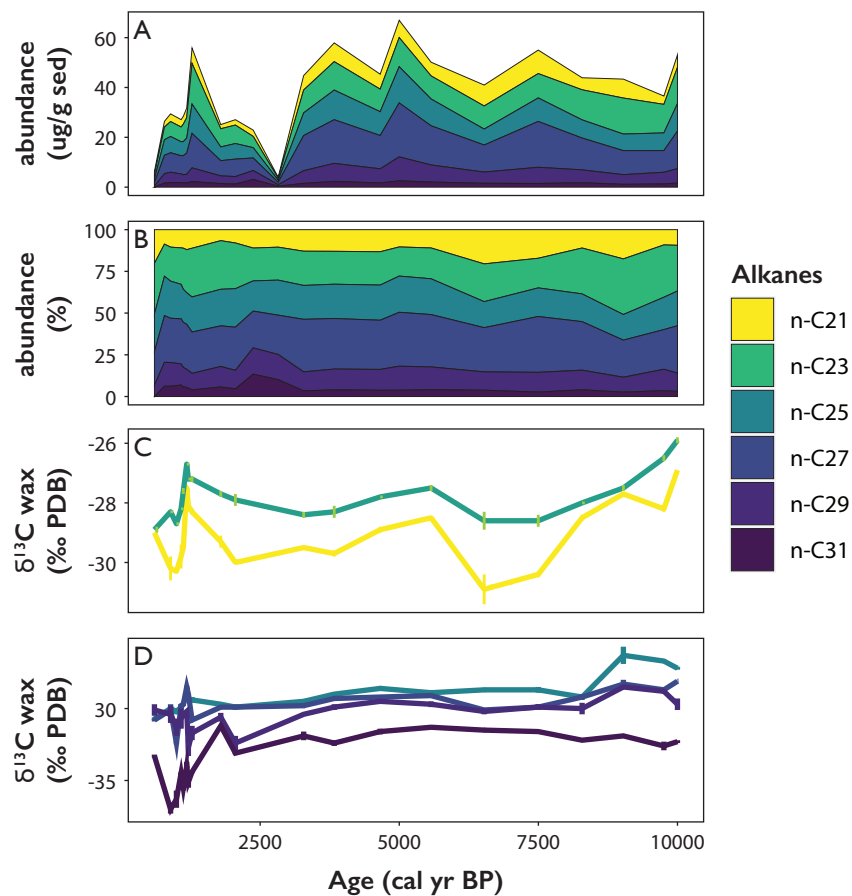
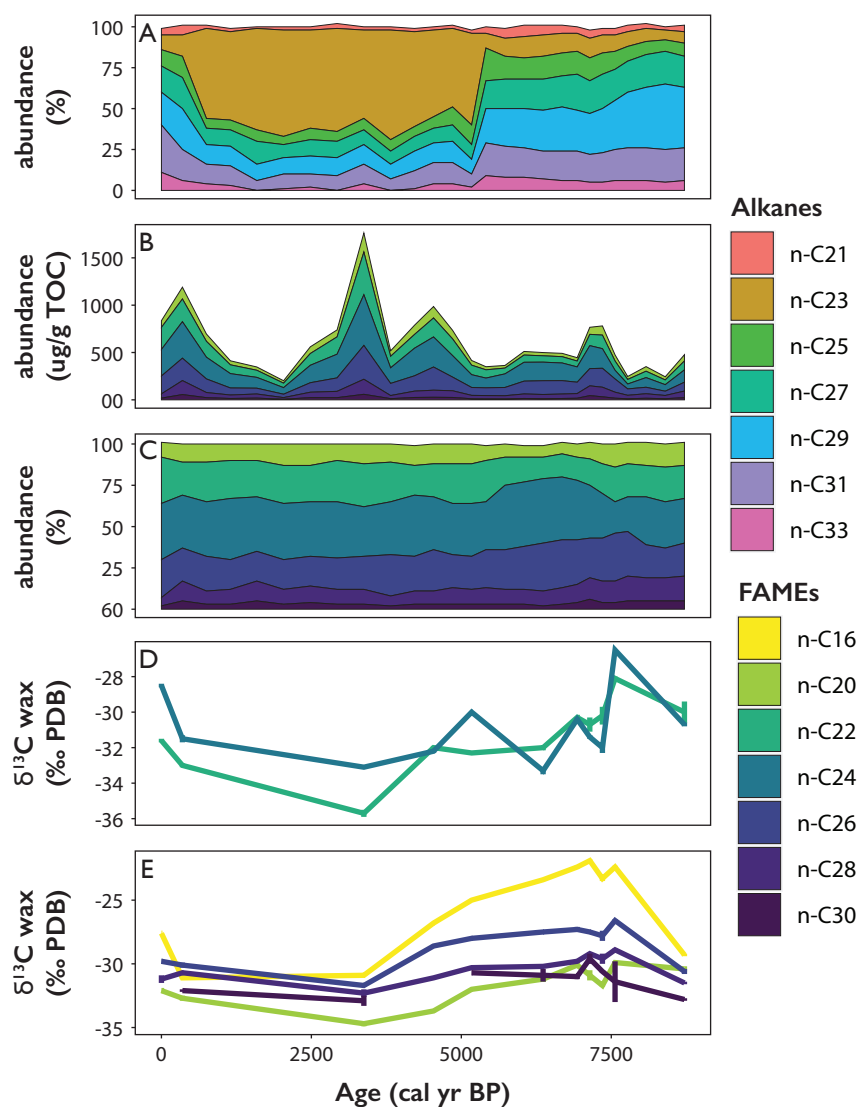


Figure S3. Wax Lips Lake Holocene sedimentary plant wax A) abundances of n-alkanes (C21-C31) in  $\mu\text{g/g}$  dry sediment, B) abundances of n-alkanes (C21-C31) as fractional abundances, C)  $\delta^{13}\text{C}$  values (‰ VPDB) of n-alkanes (C21, C23), and D)  $\delta^{13}\text{C}$  values (‰ VPDB) of n-alkanes (C25-C31).



**Figure S4.** Trifna SØ Holocene sedimentary plant wax A) abundances of n-alkanes (C21-C33) in  $\mu\text{g/g TOC}$ , B) abundances of n-alkanoic acids (C20-C30) in  $\mu\text{g/g TOC}$ , C) abundances of n-alkanoic acids (C20-C30) as fractional abundances, D)  $\delta^{13}\text{C}$  values (‰ VPDB) of n-alkanoic acids (C22, C24), and E)  $\delta^{13}\text{C}$  values (‰ VPDB) of n-alkanoic acids (C16, C20- C30).